Continuous Drive Friction Welding of Al/SiC Composite and AISI 1030

After examining the joining of a SiC particulate-reinforced A356 aluminum alloy and AISI 1030 steel, the outcome shows an aluminum matrix composite and AISI 1030 steel can be joined by friction welding

BY S. ÇELİK AND D. GÜNEŞ

ABSTRACT

In conventional welding methods, such as those used in joining ceramic-reinforced aluminum matrix composites, a variety of problems occur. For instance, the element used for reinforcement, which increases the viscosity in the melting stage, makes the mixing of matrix and reinforcement material difficult, and this causes inferior joining quality and makes the establishment of welding difficult. Also, chemical reactions and undesirable phases are observed because there is a difference between the chemical potential of the matrix and reinforcement material. In this study, joining a SiC particulate-reinforced A356 aluminum alloy and AISI 1030 steel by continuous drive friction welding was investigated. The integrity of the joints was also investigated by optical and scanning electron microscope (SEM), and the mechanical properties of the welded joints were assessed using microhardness and tensile tests. The results indicate that an aluminum matrix composite and AISI 1030 steel can be joined by friction welding.

Introduction

Recent technological advances have necessitated the development of new materials as well as new methods for joining them. An example of such a material is the metal matrix composite (MMC), which is essentially a structure consisting of a combination of two or more macro components that dissolve within one another. Metal matrix composites, which both have a high elastic modulus of ceramic and high metal ductility, are used with conventional metallic materials in fields such as aircraft and aerospace engineering, as well as defense and automotive industries. Ratios such as strength/weight and strength/density play an important role in metal matrix composites, and in so doing, they add something novel and innovative to the scope of structural materials (Refs. 1, 2).

As the demand for these new materials grows, studies related to the production and mechanical properties of composite materials have become a focus of research. Additionally, many studies about the production processes and estimation properties for this kind of material are continuing. Furthermore, investigations on practical applications of secondary processing technologies (such as machining, joining, plastic forging, etc.) are also remarkable. Currently, research related to joining science and technology for the metal matrix composites (in particular, aluminum alloy matrix composites) also becomes one of the key-point issues for their potentially successful engineering applications.

There are still many problems with joining metal matrix composite materials (in particular, for the ceramic-reinforced aluminum alloy matrix composites) used in fusion welding processes (Ref. 3).

In the welding stage, existence of the difference between the chemical potential of the matrix and reinforcement material shows there is no thermodynamic balance between the two. Under the welding conditions, undesirable chemical reactions occur between the aluminum and SiC. The result is an inferior-quality welded joint.

Uncontrolled solidification is another problem that one may encounter in fusion welding. This process occurs in the welding pool as cooled down; that is, the reinforcement phases such as SiC particulates were strongly rejected by the solidification front and normal solidification processes of the welding pool were broken down that consequently led to microsegregation or inhomogeneous distribution of reinforcement material. As a result, there would be many micro and macro defects in the welded joint (Refs. 3, 4). As there are a number of problems that may occur in the process of fusion welding, the friction welding method (a solid form welding process) proves to be more effective.

Friction welding is a method that does not cause melting in the welded zone, and it works through applying friction-induced heat on the surfaces of materials. The friction welding process is entirely mechanically powered, without any aid from electrical or other energy sources (Refs. 5, 6). In friction welding, the surfaces that create the friction during the welding process are maintained under axial pressure, known as the friction stage (Ref. 7). When the appropriate temperature is reached, the rotation movement is stopped, and the upset pressure is applied. The welding zone is thus subjected to a type of thermomechanical process that prevents grain structure deterioration (Refs. 8, 9). Friction welding is a method that can be used in materials that have different thermal and mechanical properties.

Midling and Grong (1994) were con-

KEYWORDS

Friction Welding
Weldability Testing
Metal Matrix Composite
Carbon Steel

S. ÇELİK (scelik@balikesir.edu.tr) *and D. GÜNEŞ are with Balikesir University, Faculty of Engineering and Architecture, Dept. of Mechanical Eng., Cagis Campus, Balikesir, Turkey.*

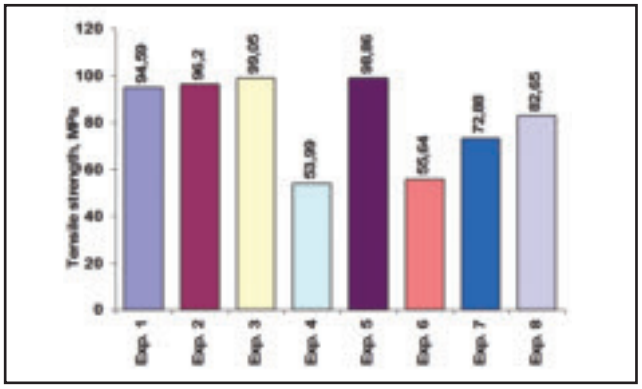

Fig. 1 — Tensile strength values of welded samples.

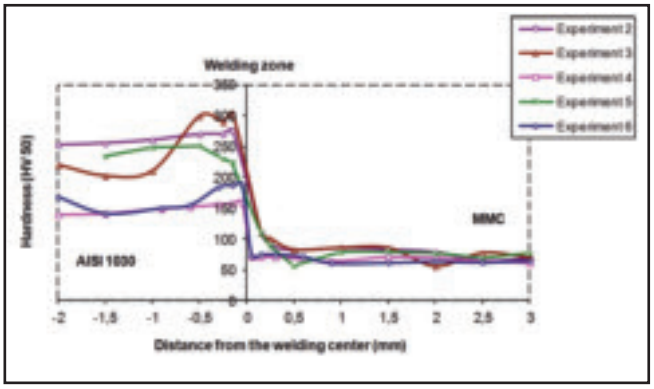

Fig. 2 — Hardness variations on horizontal distance.

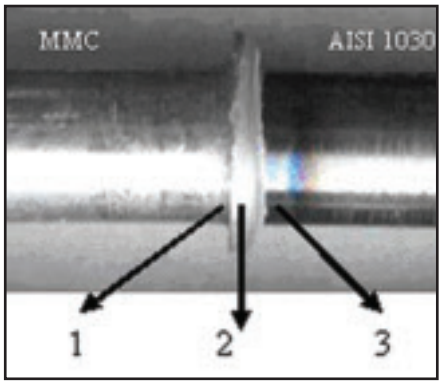

Fig. 3 — Macro picture of the sample with friction welding.

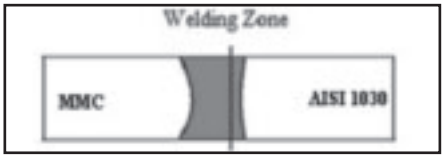

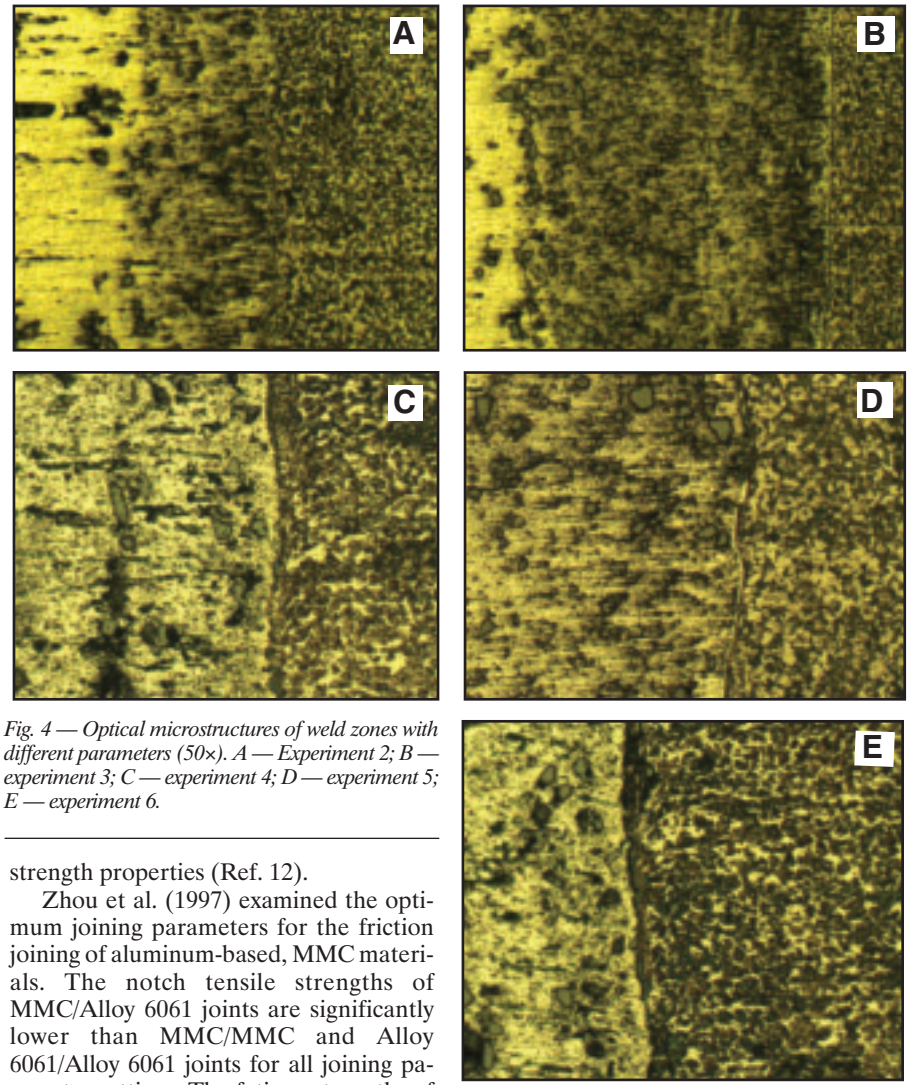

Fig. 4 — Optical microstructures of weld zones with different parameters (50×). A — Experiment 2; B — experiment 3; C — experiment 4; D — experiment 5; E — experiment 6.

cerned with the development of an overall process model for the microstructure and strength evolution during continuous-drive friction welding of AI-Mg-Si alloys and AI-SiC metal matrix composites. In Part I, the different components of the model are outlined and analytical solutions presented, which provide quantitative information about the heat-affected zone (HAZ) temperature distribution for a wide range of operational conditions. In Part II, the heat and material flow models presented in Part I are utilized for the prediction of the HAZ subgrain structure and strength evolution following welding and subsequent natural aging. The models are validated by comparison with experimental data and are illustrated by means of novel mechanism maps (Refs. 10, 11).

In their study, Pan et al. (1996) investigated the microstructure and mechanical properties of dissimilar friction joints between aluminum-based MMC and AISI 304 stainless steel base materials. The interlayer formed at the dissimilar joint interface was comprised of a mixture of oxide ($Fe(Al,Cr)_2O_4$ or $FeO(Al,Cr)_2O_3$) and $FeAl_3$ intermetallic phases. The notch tensile strength of dissimilar MMC/AISI 304 stainless steel joints increased when the rotational speed increased from 500 to 1000 rev/min, and at higher rotation speeds there was no effect on notch tensile strength properties (Ref. 12).

Zhou et al. (1997) examined the optimum joining parameters for the friction joining of aluminum-based, MMC materials. The notch tensile strengths of MMC/Alloy 6061 joints are significantly lower than MMC/MMC and Alloy 6061/Alloy 6061 joints for all joining parameter settings. The fatigue strengths of MMC/MMC joints and Alloy 6061/6061 joints are also poorer than the as-received base materials (Ref. 13).

Uenishi et al. (2000) investigated spiral defect formation and the factors affecting the mechanical properties of friction welded aluminum Alloy 6061 T6 and 6061/AI_20_3 composite base materials. Spiral defects are flow-induced defects formed when material and reinforcing

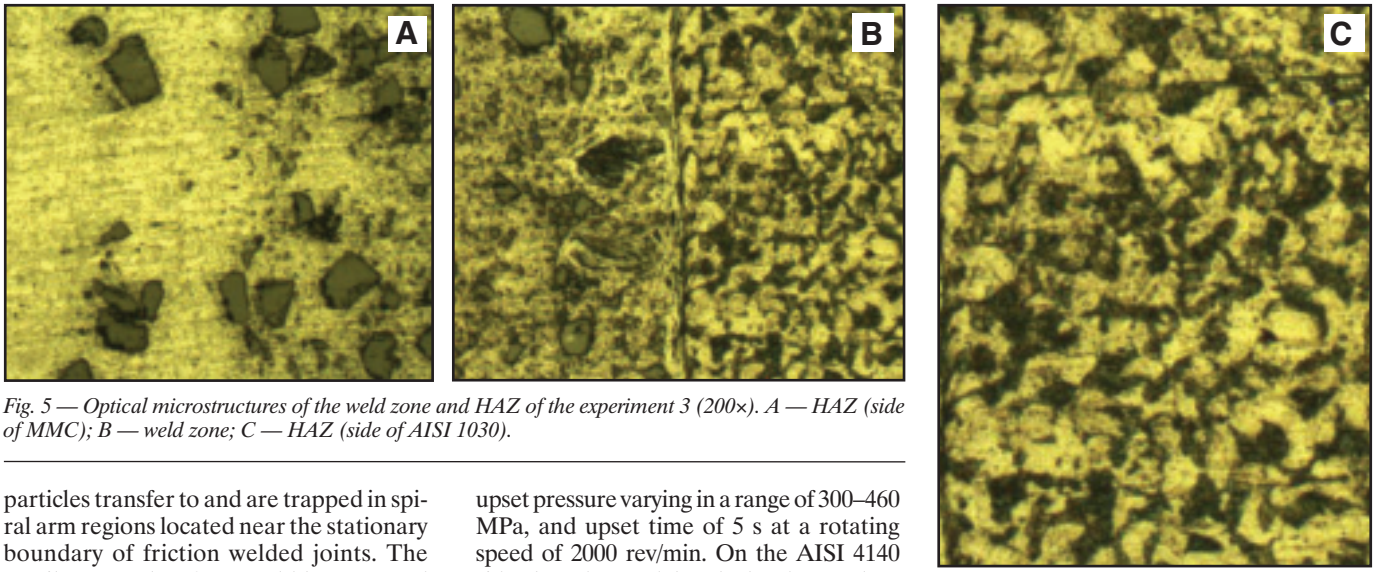

Fig. 5 — Optical microstructures of the weld zone and HAZ of the experiment 3 (200×). A — HAZ (side of MMC); B — weld zone; C — HAZ (side of AISI 1030).

particles transfer to and are trapped in spiral arm regions located near the stationary boundary of friction welded joints. The tensile strengths of postweld heat treated MMC/MMC joints produced using a friction pressure of 280 MPa were significantly stronger than as-received MMC base material (Ref. 14).

In their study, Lin et al. (2002) were able to successfully conduct friction welding between two composite materials with the same matrix but a different reinforced material. Composite materials are SiC and Al_2O_3 reinforced A7005 aluminum alloy. For composite materials, the following were used: size 6 and 15 μm, SiC particulate volume percentage of 10%, and 15 μm Al_2O_3 ceramic particulate of the same volume percentage. Consequently, the use of a SiC particulate led to a concentration of reinforcement particulate in the HAZ. This results in an increase in hardening values in the plastic region, weakening welding strength, and narrowing HAZ (Ref. 15).

Lee et al. (2004) were able to achieve friction welding between a TiA1 alloy and AISI 4140 for a friction time of 30–50 s, upset pressure varying in a range of 300–460 MPa, and upset time of 5 s at a rotating speed of 2000 rev/min. On the AISI 4140 side, they observed that the hardness values increased to the range of 600–900 HV, and no change in the TiA1 hardness value. However, the tensile strength value was determined to be as low as 120 MPa (Ref. 16).

Reddy et al. (2008) were able to successfully weld AA6061 and AISI 304 austenitic stainless steel by means of the continuous rotating friction welding method. Direct welding of this combination resulted in brittle joints due to the formation of Fe_2Al_5. To alleviate this problem, welding was carried out by incorporating Cu, Ni, and Ag as a diffusion barrier interlayer. The interlayer was incorporated by electroplating. Welds with a Cu and Ni interlayer were also brittle due to the presence of $CuAl_2$ and $NiAl_3$. Ag acted as an effective diffusion barrier for Fe avoiding the formation of Fe_2Al_5. Therefore, welds with an Ag interlayer were stronger and ductile (Ref. 17).

In the study by Fauzi et al. (2010), the examination of the interface with ceramic/metal alloy friction welded components is essential for understanding the quality of bonding between two dissimilar materials. Optical and electron microscopy as well as four-point bending strength and microhardness measurements were taken to evaluate the quality of bonding alumina and 6061 aluminum alloy joints produced by friction welding (Ref. 18).

In this study, the joining capability of SiC_p-reinforced A356 aluminum matrix composite and AISI 1030 steel was studied by continuous-drive friction welding. Therefore, after welding of samples, tensile and hardness experiments were carried out. For metallographic investigations, optical microscope and SEM have been used. Energy-dispersive spectroscopy (EDS) analysis was carried out for chemical composition investigations on welding and HAZs.

Experimental Procedure

In this study, SiC_p-reinforced A356 aluminum matrix composite and AISI 1030 steel were used. A SiC particulate-reinforced A316 aluminum matrix composite was prepared using the vortex method. In the Al/SiC composite material, some reactions take place between the matrix and reinforcement material during casting. The Al_4C_3, which formed as a result of these reactions, renders the welding very brittle. Very high heat input makes Al_4C_3 even more pronounced. The compound takes form at a temperature between 700° and 1400°C (Refs. 1, 19). To prevent brittleness of the composite material caused by the Al_4C_3 compound, the vortex method that does not require very high heat input is used. The casting was carried out using the stir casting method at 700°C.

The chemical composition of the A356 aluminum alloy is presented in Table 1. It should be noted that the SiC particulate

Table 1 — Chemical Composition of the A356 Material (wt-%)

Al	Fe	Si	Ti	Mn	Zn	Cu	Mg	Ni	Cr
92.28	0.12	7	0.2	0.03	0.02	0.02	0.28	0	0

Table 2 — Chemical Composition of the AISI 1030 Steel (wt-%)

C	Ni	Cr	Si	Mn	P	Cu	Mo	Nb	Fe
0.297	0.100	0.082	0.143	0.636	0.011	0.167	0.011	<0.002	98.511

Table 3 — Mechanical Properties of the Base Materials

Materials	Yield Strength (MPa)	Tensile Strength (MPa)	Elongation (%)	Hardness (HV50)
AISI 1030	477.68	725.46	5.20	232.3
6% Al/SiCp	103.76	149.57	0.025	64.5

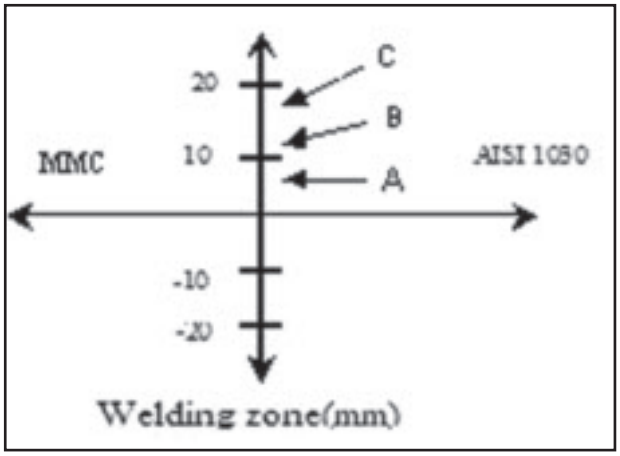

Fig. 6 — The points where SEM images were taken.

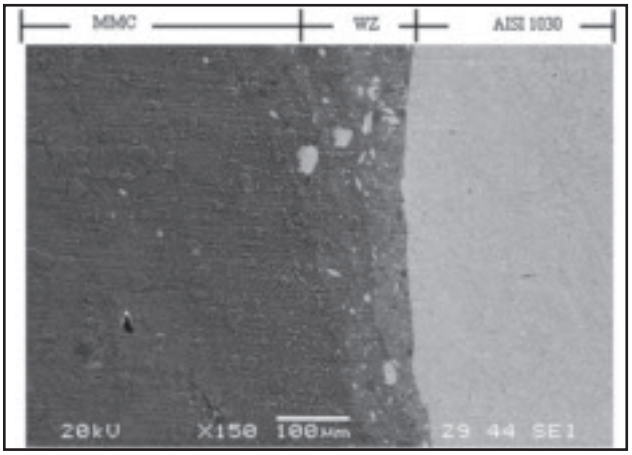

Fig. 7 — SEM image of point A.

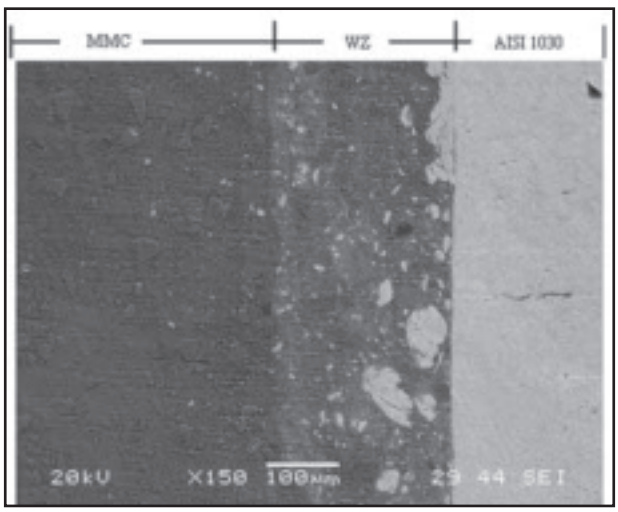

Fig. 8 — SEM image of point B.

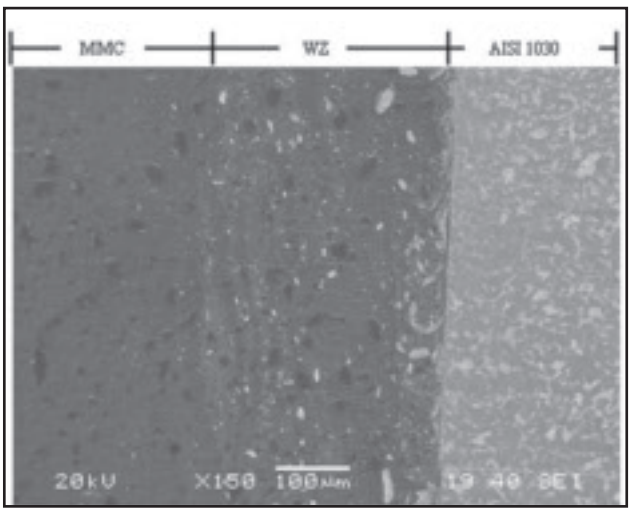

Fig. 9 — SEM image of point C.

volume percentage of 6% in 44 µm dimensions were used in the study. Looking to the related literature (Ref. 20) and the results of a number of preliminary castings, it was assumed that 6% SiC would be the appropriate particulate ratio to use. The chemical composition of AISI 1030 steel is shown in Table 2. Mechanical properties of this steel are presented in Table 3. The samples were processed at ∅20 × 80 mm dimensions for friction welding.

The study was conducted using a continuous-drive friction welding machine at 3000 rev/min at the Engineering and Architecture Faculty of Balikesir University. Surfaces of the joining parts were ground, cleaned, and then fixed to the machine. The welding parameters, which were determined after consulting the relevant literature (Refs. 15, 20, 21) and preliminary experiments, are shown in Table 4.

Tensile properties of the welded samples were prepared according to the EN 895 standard by leaving the welding zone in the center. When running tensile tests, 4-mm/min tensile rates were used. Hardness tests were carried out in the cross-section interface of the Al/SiC composite and AISI 1030 steel friction welded joints. The microhardness values were measured on both sides of the welded specimens with the Vickers method using a 50-g load.

The microstructural features of the friction welded joints are investigated by using optical and scanning electron microscopes. The samples were ground by using SiC sandpapers and polished with a 0.3-µm Al_2O_3 powder, then AISI 1030 and MMC sides were etched by using different solutions. The AISI 1030 was etched for 4 s by using 4% nital, while the %6 Al/SiCp material was etched for 2 min using a Keller reagent (2.5 mL HNO_3, 1.5 mL HCI, 1 mL HF, and 95 mL distilled water).

Results and Discussion

Tensile Test Results

Friction welding experiments were conducted using the aforementioned welding parameters. In the tensile test samples, fractures occurred on the side of the MMC material in the HAZ. The occurrence of fractures in the MMC zone was apparently

Table 4 — The Process Parameters Used in the Friction Welding Experiments

Experiment No.	Friction Pressure (P_f) (MPa)	Friction Time (t_f) (s)	Upset Pressure (P_u) (MPa)	Upset Time (t_u) (s)
Experiment 1	40	4	40	4
Experiment 2	40	6	40	4
Experiment 3	40	10	40	4
Experiment 4	20	6	40	4
Experiment 5	20	12	40	4
Experiment 6	20	4	60	4
Experiment 7	20	6	60	4
Experiment 8	20	8	60	4

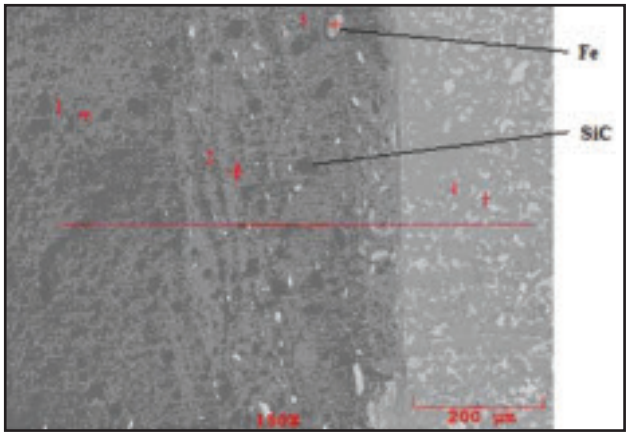

Fig. 10 — EDS analysis line and points on experiment 3.

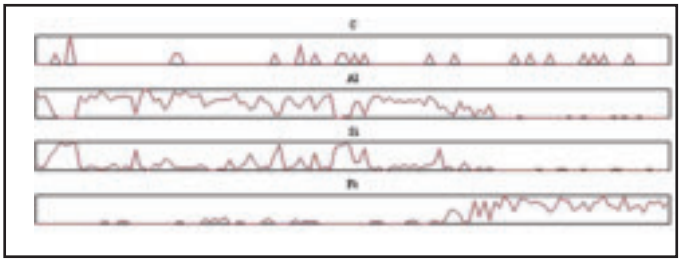

Fig. 11 — Linear EDS analysis results of the weld zone.

caused by a deficiency of connection, which is a reduced microjoining interface between SiC_p and A356 aluminum. On the other hand, the reason that a fracture took place in the welding zone could be attributed to the presence of intermetallic phases such as Fe_2Al_5 and $FeAl_3$, which resulted from the diffusion of materials. This was caused by mechanical locking of the MMC and AISI 1030 materials, but it could also be the impact of SiC_p, which prevented diffusion of the materials, the fact that Al and Fe promote the intermetallic phases (Refs. 12, 17, 22, 23).

The tensile test results of the friction-welded joints are given in Fig. 1 in a bar chart format. According to the results of the tensile tests, the tensile strength of the sample from experiment 3 (99.05 MPa) is 33.7% less than the tensile strength of MMC (1349.57 MPa), while the tensile strength of the sample used in experiment 4 (53.99 MPa) is 63.9% less than the tensile strength of MMC. In general, the tensile strength of materials used in friction welding must be close to that of the material with the lowest tensile strength. In the tests, the tensile strength of the welded zone was determined even lower than that of MMC material, which has the lowest strength. This can be explained that the lack of strong interface connection strength between the reinforcement material and matrix material, and acting of SiC_p as a gap in the welding zone reduces the welding strength.

It can be concluded that the friction welding parameters are effective on joint strength. With a long friction time, zones of diffusion containing brittle intermetallic components were formed. A connection could not be established with a short period of friction time and low friction rate with upset pressure. To obtain high strength, the friction time must be as short as possible, while friction and upset pressure levels remain high. In short periods of friction time, a very small diffusion area forms, and this zone is removed from the joining interface by means of pressure during the welding process in which upset pressure is exerted. The results matched the data in previously conducted studies (Refs. 21, 23).

Microhardness Test Results

When looking at the hardness graph in Fig. 2, it is clear that hardness values change when moving away from the welding zone and toward the main materials. This change continues until the hardness values of the main materials are reached. On the MMC side, where particle fracture occurred, the increase in hardness values begins as a more particulate concentrate in the unit area, and it reaches its maximum level on the steel side of the weld zone. Five of the test samples with high tensile strength were examined for microhardness, and the results are provided in Fig. 2.

In experiments 2, 3, and 5, high pressure and a long period of friction led to an increase in intermetallic phases with resulting deformation. This created an expansion of the weld zone. It is observed that deformation hardening, intermetallic phases originating from iron, aluminum, and fracturing of SiC increased the hardness in the region that deformed and near to the weld zone (Ref. 24). It is possible that there were particle transitions in the viscose structure of these samples due to the upset and heat. It should also be noted that a part of Fe passes to the side of MMC during welding, while Al and Si pass to the side of AISI 1030 and accumulate in the weld zone, causing an increase in hardness. These transitions were determined by an EDS analysis, which is explained in a subsequent section. Due to the fact that the friction time of test samples was less than 10 s, the occurrence of higher hardness values, which could cause weaker welding strength, was prevented.

In experiments 4 and 6, it was observed that the friction and upset pressures were low while the weld zone between MMC and AISI 1030 materials was narrower than it ought to be. Because of this, diffusion between the materials could not be achieved. This was due to the fact that the friction pressure and time were not sufficient for the materials to diffuse, and the joint between the two materials was very slight. The highest hardness values of the weld zone were measured at the sample of experiment 3, while the sample from experiment 4 showed the lowest microhardness values. It was observed that friction time and pressure values have a direct effect on microhardness values.

Macro- and Microstructure Results

The structural changes taking place when welding two different materials can be classified into three different areas. The first of these shows the partially deformed section of MMC, while the second shows the fully deformed section in the weld center, and the third shows the partially deformed zone of AISI 1030 — Fig. 3.

In examining the microstructure, it was observed that there were changes in the particle structure of the MMC material, whereas not much change took place in the AISI 1030 material. The reason no change occurred on the AISI 1030 side was the low friction pressure and time.

In general, due to the effects of friction and upset pressure, fracture in the SiC particulate was observed in the MMC material when approaching the weld zone. This phenomenon led to deposits of SiC in the weld zone. Uenishi et al. (Ref. 14) reported that reinforcing Al_2O_3 particles in the MMC base material are fractured in the zone close to the weld interface. After samples were examined under an optical microscope, it became easier to explain why the hardness values in the weld zone increased at higher pressure and time. Moreover, the occurrence of Al-Fe intermetallic phases is expected as a result of heat generated by the friction as well as upset pressure. In the literature (Refs. 12, 17, 22, 23), it has been claimed that intermetallic phases between Al and Fe such as Fe_2Al_5 and $FeAl_3$ can take place after the diffusion of the materials under high pressure if a sufficient amount of heat (at higher than 400°C) is provided. The subject material's intermetallic phases adversely affect the weld strength because they form a brittle structure. To prevent this,

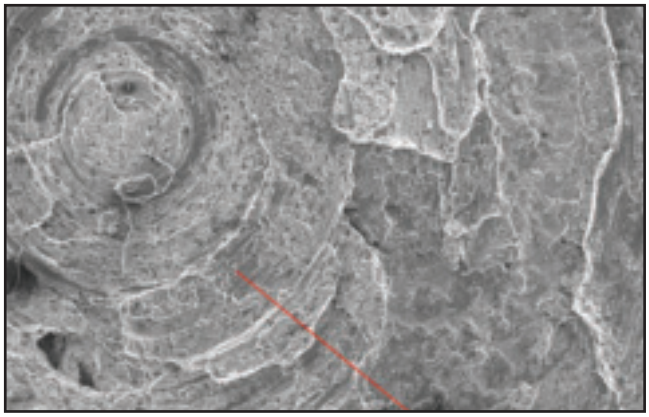

Fig. 12 — SEM image of fracture surface on the side of AISI 1030 material and EDS analysis line.

there must be high friction and upset pressure, as well as sufficient friction time mentioned before.

Figure 4 depicts the microstructure images of samples in five different experimental conditions. In examining samples 4 and 6, it can be observed that the welding is like a line, and the zone of transition where the materials diffuse into each other is not revealed. In visual and microscopic examinations of the samples, it was observed that flange and weld zones were not formed. It was also observed that the materials were connected only by means of mechanical locking, and there was no diffusion between the materials due to the fact that the necessary friction temperature could not be achieved with the insufficient friction pressure and time.

The joining quality of the samples from experiments 2, 3, and 5 was very good, especially as the width of the weld zone can easily be seen. It can further be seen from MMC that the materials are sufficiently diffused to ensure joining. The diffusion between the materials as well as the formation of the weld zone was adequately achieved due to the high pressure and sufficient friction. Detailed microstructural images belong to the zones 1, 2, and 3 depicted in Fig. 3 are shown respectively in Fig. 5A–C.

In the friction welding process, circular velocity is zero at the center. As the diameter and distance from the center increases, this velocity increases. In connection with this, friction and temperature rise. Moreover, the width of the HAZ gets larger (Refs. 24–26). These changes were investigated throughout the welded area at various recorded distances from the welding center. Deeply assessed points of A, B, and C in the welded joint are depicted in Fig. 6, and SEM images of these points taken from the welded joint zone are shown in Figs. 7–9. Following the SEM investigation, a linear EDS analysis of zone C was carried out. In Fig. 10, the lines and points used in the EDS analysis are revealed, and Fig. 11 depicts the results. In Table 5, values obtained from point analysis can be seen.

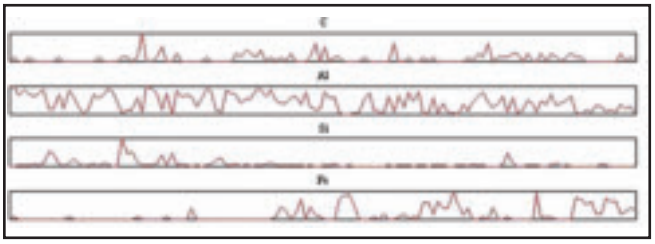

Fig. 13 — Linear EDS analysis results of fracture surface on the side of AISI 1030 material.

Examining the SEM images and EDS results, the distribution of Al, SiC_p, and Fe can be seen in the weld zone. In the weld zone, it can be observed that the Fe element is more diffused on the side of the MMC while Al and SiC_p were not very diffused on the AISI 1030 side. On the side of MMC, as the weld zone is approached, the size of the SiC particulate became smaller; in other words, they were broken. As was previously explained, microhardness values in the weld zone increase as the amount of particulate in each unit zone increases, which in itself is caused by the fracture of SiC particulate that accumulated in the weld zone. In the SEM images, SiC_p clustering in the weld zone was not observed. This supports the results that the weld strength in this sample is high.

When examining the fracture surfaces more closely, we can see smooth and bright surfaces that mean it is a brittle fracture. In Fig. 12, it can be observed that there were many indentations on the surface in the form of white braids that resulted from the tensile force that was applied. Also, there were large dents with ductile fractures prevalent in these sections of the material.

To be able to understand the Fe, SiC_p, and Al status on the fracture surface, a linear EDS analysis was taken on the AISI 1030 — Fig. 12. The results of the linear analysis are shown in Fig. 13. The fact that SiC, Al, and Fe materials are on the same surface and also that there are remains of MMC material on the fracture surface indicate the fracture took place on the MMC side close to the welding zone.

Conclusions

1. In the tensile tests applied to the welded samples, it was observed that experiment 3 had the highest tensile strength (99.05 MPa), whereas experiment 4 had the lowest tensile strength (53.99 MPa). It was observed that friction pressure and friction time were important for welding strength. Friction pressure has to be at the optimum value where it does not cause high deformation but still allows for diffusion.

2. In the examinations of hardness performed on the welded samples, hardness values are not linear, also they increase while moving away from the welded zone toward the main materials. The increase in hardness values in the welded zone is the result of intermetallic phases such as Fe_2Al_5 and $FeAl_3$, internal stress generating by high temperature differences, deformation hardening, and fracturing of SiC_p because of high pressure in the zone.

3. In the microstructural examinations performed on the weld zone, three separate zones were encountered: the HAZ side to the MMC; the weld zone (deformed after being exposed to high temperature values); and the HAZ side to AISI 1030. Substantial structural change was not observed in the HAZ side to AISI 1030. This is due to the fact that the temperature did not reach sufficient values for the deformation of AISI 1030 during friction welding.

4. In investigating the SEM images, the diffusion of SiC_p, Al, and Fe were observed in the weld zone. It was also noted that as SiC was located closer to the weld

Table 5 — EDS Analysis Values Obtained from Points in Fig. 10

Element	(1) wt-%	(2) wt-%	(3) wt-%	(4) wt-%
C K	—	—	—	4.763
O K	8.770	—	—	—
Al K	56.328	78.551	—	—
Si K	34.902	5.702	—	0.193
Fe K	—	15.747	100.000	94.326

zone, it fractured, and its size diminished due to the effect of upset pressure. This, in turn, caused an increase in plastic deformation and to rise in the hardness value.

5. According to the tensile and hardness tests and the microstructure, SEM and EDS investigations, the best welding parameters were in experiment 3 (P_f = 40 MPa, P_u = 40 MPa, t_f = 10 s, t_u = 4 s). At locations where MMC and AISI 1030 have to be used together, the use of friction welding as a joining method resulted in the realization of the welding in a very short time by working below melting temperatures. More specifically, it has shown that SiC-reinforced A356 aluminum alloy can be successfully joined to AISI 1030 steel by friction welding.

References

1. Zhu, Z. A. 1988. Literature survey on fabrication methods of cast reinforced metal composites. Edited by S. G. Fishman and A. K. Dhingra. ASM/TMS Committee, World Materials Congress, Sept. 24–30, Chicago, Ill.

2. Han, N. L., Yang, J. M., and Wang, Z. G. 2000. Role of real matrix strain low cycle fatigue life of a SiC particulate reinforced aluminum composite. *Scripta Mater.* 43: 801–5.

3. Zhang, X. P., Quan, G. F., and Wei, W. 1999. Preliminary investigation on joining performance of SiC-reinforced aluminum metal matrix composite by vacuum brazing. *Composites* Part A 30: 823–7.

4. Zhang, X. P., Ye, L., Mai, Y. W., Quan, G. F., and Wei, W. 1999. Investigation on diffusion bonding characteristics of SiC particulate reinforced aluminum MMC. *Composites* Part A 30: 1415–21.

5. Meshram, S. D., Mohandas, T., Madhusudhan, and Reddy, G. 2008. Friction welding of dissimilar pure metals. *J. Mater. Process Tech.* 184: 330–7.

6. 1980. Resistance and solid-state welding and other joining processes. *Welding Handbook*, p. 240. Miami, Fla.: AWS.

7. Spindler, D. E. 1994. What industry needs to know about friction welding. *Welding Journal* 73(3): 37–42.

8. Boyer, H. E., and Gall, T. L. 1988. Joining, desk edition. *Metals Handbook*, pp. 30–58. Metals Park, Ohio.

9. Jenning, P. 1971. Some properties of dissimilar metal joints made by friction welding. *The Welding Institute*, pp. 147–53. Abinghton Hall, Cambridge.

10. Midling, O. T., and Grong, O. 1994. A process model for friction welding of A1-Mg-Si alloys and Al-SiC metal matrix composites — I. HAZ temperature and strain rate distribution. *Acta Metall. Mater.* 42(5): 1595–1609.

11. Midling, O. T., and Grong, O. 1994. A process model for friction welding of A1-Mg-Si alloys and Al-SiC metal matrix composites — I. HAZ microstructure and strength evolution. *Acta Metall. Mater.* 42(5): 1611–22.

12. Pan, C., Hu, L., Li., Z., and North, T. H. 1996. Microstructural features of dissimilar MMC/AISI 304 stainless steel friction joints. *J. Mater. Sci.* 32: 3667–74.

13. Zhou, Y., Zhang, J., North, T., and Wang, H. Z. 1997. The mechanical properties of friction welded aluminum-based metal-matrix composite materials. *J. Mater. Sci.* 32: 3883–89.

14. Uenishi, K., Zhai, Y., North, T. H., and Bendzsak, G. J. 2000. Spiral defect formation in friction welded aluminum. *Welding Journal* 79(7): 184-s to 93-s.

15. Lin, C. B., Chou, C., and Ma, C. L. 2002. Manufacturing and friction welding properties of particulate reinforced 7005 Al. *J. Mater. Sci.* 37: 4645–52.

16. Lee, W. B., Kim, M. G., Koo, J. M., Kim, K. K., Quesnel, D. J., Kim, Y. J., and Jung, S. B. 2004. Friction welding of TiAl and AISI 4140. *J. Mater. Sci.* 39: 1125–8.

17. Reddy, M. G., Rao, S. A., and Mohandas, T. 2008. Role of electroplated interlayer in continuous drive friction welding of AA6061 to AISI 304 dissimilar metals. *Science and Technology of Welding & Joining* 13(7), October: 619–28.

18. Fauzi, M. N. A., Uday, M. B., Zuhailawati, H., and Ismail, A. B. 2010. Microstructure and mechanical properties of alumina-6061 aluminum alloy joined by friction welding. *Materials and Design* 31: 670–67.

19. Durmuş, H., and Meriç, C. 2009. Weldability of Al99–SiC composites by CO_2 laser welding. *Journal of Composite Materials* 43: 1435–50.

20. Lin, C. B., Mu, C. K., Wu, W. W., and Hung, C. H. 1999. The effect of joint design and volume fraction on friction welding properties of A360/SiC(p) composites. *Welding Journal* 78(3): 100–8.

21. Lienert, T. J., Baeslack, W. A., Ringnalda, J., and Fraser, H. L. 1996. Inertia-friction welding of SiC-reinforced 8009 aluminum. *J. Mater. Sci.* 31: 2149–57.

22. Peyre, P., Sierra, G., Deschaux-Beaume, F., Stuart, D., and Fras, G. 2007. Generation of aluminum-steel joints with laser-induced reactive wetting. *Mater. Sci. and Eng. A* 444: 327–38.

23. Naoi, D., and Kajihara, M. 2007. Growth behavior of Fe_2Al_5 during reactive diffusion between Fe and Al at solid-state temperatures. *Materials Sci. and Eng. A* 459: 375–382.

24. Li, Z., Maldonado, C., North, T. H., and Altshuller, B. 1997. Mechanical and metallurgical properties of MMC friction welds. *Welding Journal* 76(9): 367–73.

25. Noh, M. Z., Hussain, L. B., and Ahmad, Z. A. 2008. Alumina-mild steel friction welded at lower rotational speed. *J. Mater. Process Tech.* 204: 279–83.

26. Çelik, S., and Ersözlü, I. 2009. Investigation of the mechanical properties and microstructure of friction welded joints between AISI 4140 and AISI 1050 steels. *Materials and Design* 30: 970–6.

CAN WE TALK?

The *Welding Journal* staff encourages an exchange of ideas with you, our readers. If you'd like to ask a question, share an idea or voice an opinion, you can call, write, e-mail or fax. Staff e-mail addresses are listed below, along with a guide to help you interact with the right person.

Publisher
Andrew Cullison
cullison@aws.org, ext. 249
Article Submissions

Editor
Mary Ruth Johnsen
mjohnsen@aws.org, ext. 238
Feature Articles

Associate Editor
Howard Woodward
woodward@aws.org,ext. 244
Society News, Personnel

Associate Editor
Kristin Campbell
kcampbell@aws.org, ext. 257
New Products
News of the Industry

Managing Editor
Zaida Chavez
zaida@aws.org, ext. 265
Design and Production

Sr. Production Coordinator
Brenda Flores
bflores@aws.org, ext. 330
Production

Advertising Sales Director
Rob Saltzstein
salty@aws.org, ext. 243
Advertising Sales

Advertising Sales & Promotion Coordinator
Lea Paneca
Lea@aws.org, ext. 220
Production and Promotion

Sr. Advertising Production Manager
Frank Wilson
fwilson@aws.org, ext. 465
Advertising Production

Peer Review Coordinator
Melissa Gomez
mgomez@aws.org, ext. 475
Peer Review of Research Papers

Welding Journal Dept.
550 NW LeJeune Rd.
Miami, FL 33126
(305/800) 443-9353
FAX (305) 443-7404